Eur. Phys. J. C (2025) 85:741
https://doi.org/10.1140/epjc/s10052-025-14431-3

THE EUROPEAN PHYSICAL JOURNAL C

Regular Article - Theoretical Physics

Testing regular black holes in the framework of asymptotically safe gravity using particle dynamics, QPOs, and shadow constraints

G. Mustafa[1,2,a], **Asalkhon Alimova**[3,4,b], **Farruh Atamurotov**[5,6,7,c], **Awad A. Ibraheem**[8,d], **Phongpichit Channuie**[9,10,e], **Gunel Bahaddinova**[2,f]

[1] Department of Physics, Zhejiang Normal University, Jinhua 321004, People's Republic of China
[2] Research Center of Astrophysics and Cosmology, Khazar University, 41 Mehseti Street, 1096 Baku, Azerbaijan
[3] New Uzbekistan University, Movarounnahr street 1, 100000 Tashkent, Uzbekistan
[4] Tashkent State Technical University, 100095 Tashkent, Uzbekistan
[5] Kimyo International University in Tashkent, Shota Rustaveli str. 156, Tashkent 100121, Uzbekistan
[6] Inha University in Tashkent, Ziyolilar 9, Tashkent 100170, Uzbekistan
[7] University of Tashkent for Applied Sciences, Str. Gavhar 1, Tashkent 100149, Uzbekistan
[8] Department of Physics, Faculty of Science, King Khalid University, Abha, Saudi Arabia
[9] School of Science, Walailak University, Nakhon Si Thammarat 80160, Thailand
[10] College of Graduate Studies, Walailak University, Nakhon Si Thammarat 80160, Thailand

Received: 8 January 2025 / Accepted: 6 June 2025

Abstract We investigate the motion of neutral test particles around a non-rotating regular black hole within the framework of asymptotically safe gravity, analyzing the impact of the black hole's parameters on particle motion. This black hole solution is characterized by an additional parameter, η, which differentiates it from the standard Schwarzschild black hole solution. We obtain analytical formulations for the energy and angular momentum of equatorial circular orbits as functions of the black hole parameter. The stability of these circular orbits is examined by the effective potential. Additionally, we present a graphical study of the innermost stable equatorial circular orbits as functions of the black hole parameter and investigate the effective force exerted on circular orbits. We also derive the frequencies of radial and latitudinal harmonic oscillations as functions of the model parameters and discuss the key features of quasi-periodic oscillations of test particles near stable circular orbits in the black hole's equatorial plane. The phenomenon of periastron precession is also considered. Additionally, we explore particle collisions near the black hole and demonstrate that such collisions can produce high energy near the event horizon. Our findings indicate that the black hole parameter significantly influences the motion of test particles around a regular black hole in the context of asymptotically safe gravity. We examine the shadow of black hole and using observational data from the Event Horizon Telescope (EHT) collaboration for Sgr A* and M87*, we have determined the range of η parameter that corresponds to the observations.

1 Introduction

Black holes (BHs) are unusual cosmic entities with enormous gravitational forces. Typically, nothing escapes a BH's event horizon due to its enormous gravitational attraction, which absorbs everything within its domain. These thermodynamic objects not only exhibit extraordinary classical characteristics but also improve our understanding of quantum gravitational phenomena. Curvature singularities are found behind the event horizons of the most well-investigated BH configurations. Regular black holes are those that prevent singularities from approaching their horizons. These BHs are particularly beneficial in high-energy collisions and need finite amounts of energy to create. Bardeen [1] proposed a regular BH model by analyzing the collapse of electrically charged matter with an Ads core within the BH, which replaced the singularity. Subsequently, several regular BH models have been developed using alternative matter sources [2–6] or in different gravity theories [7–11]. Similar efforts have been

[a] e-mail: gmustafa3828@gmail.com
[b] e-mail: asalkhon.alimova@yahoo.com
[c] e-mail: atamurotov@yahoo.com
[d] e-mail: awad_ah_eb@hotmail.com
[e] e-mail: phongpichit.ch@mail.wu.ac.th (corresponding author)
[f] e-mail: gbahaddinova@khazar.org

Published online: 04 July 2025

attempted to include quantum corrections, at least from a phenomenological point of view [12–14], or by singularity regularization [15].

In addition, a significant focus has been placed on the idea of asymptotic safety [16,17]. Recently, Bonanno et al. [17] introduced a novel model of a regular BH inspired by the theories of Markov and Mukhanov, employing the notion of gravity's anti screening properties in ultra-Planckian energy regimes. They provided a detailed metric characterizing the outside of the collapsing dust sphere within the context of asymptotically safe gravity. It is presumed that quantum adjustments, which obscure the singularity within a BH, operate on Planck scales and are unlikely to generate discernible astrophysical impacts since, far from the event horizon, the BH's geometry resembles Schwarzschild. Consequently, a natural inquiry emerges as to how these quantum modifications can be potentially detectable. The detection of black hole shadows [18] and recent detections of gravitational wave emissions from stellar-mass black hole mergers [19] provide a chance to examine intricate gravitational phenomena specific to compact relativistic entities, thereby generating new avenues for fundamental physics inquiry [20]. In this context, numerous investigations have investigated the quasi normal modes [21] and black hole shadows [22] of various ordinary black holes.

In astrophysics, the motion of particles, whether test particles or charged/neutral particles around a BH, is crucial. In addition to helping explain energetic processes that take place close to the event horizon of a BH, this study offers important insights into the large-scale structure of spacetime [23–31]. These phenomena encompass the emission of jets (arising from particle ejection in a magnetic field), accretion disks (particles orbiting the black hole), and the acceleration of cosmic rays and gamma rays. The acceleration of cosmic and gamma rays is a vital area of investigation in astronomy, with active galactic nuclei serving as primary candidates for the acceleration of ultra-high-energy cosmic rays [32,33]. Examining particle dynamics in curved spacetime enhances our understanding of spacetime characteristics. There is a great deal of literature on particle motion around many types of BHs, including brane-world BHs [34,35], quantum corrected BHs [36,37], anti-de Sitter BHs [38,39], Schwarzschild MOG BHs [40] and Kerr MOG BHs [41].

We investigate a normal black hole's shadow in asymptotically safe gravity. Under little perturbations, photons on unstable orbits either fall into the black hole or escape to infinity, creating the black hole shadow. The shadow is formed by these photons' creation of light rings that are projected onto an observer's screen. Strong gravitational lensing causes the light beams to travel close to the event horizon, making the shadow an important indicator of strong field gravity. Prominent studies by Synge [42] and Luminet [43] defined the Schwarzschild black hole shadow and determined the angular radius of photons. This was extended to spinning Kerr black holes to demonstrate how rotation distorts the shadow in Bardeen's study [44]. Research indicates that the shadows of various types of black hole can be used to evaluate gravitational theories and elucidate black hole properties. There has been a rise in both analytical and numerical investigations, as well as observational studies, regarding the shadows cast by different forms of black holes, for example [45–55]. Numerous studies have been conducted in this domain, including those derived from literary works [56–63].

Black holes possess the capacity to operate as particle accelerators [64]. Collisions between particles, including substantial dark matter (DM) particles, can attain exceptionally high center of mass energies. Although it may appear logical that particles experience limitless blue-shifting near the event horizon (from the viewpoint of an observer situated there), the center of mass between two particles exists in a free-fall frame where energy is limited. For Schwarzschild BHs, the maximum center of mass energy is given by $E_{\rm cm}^{\rm max} = 2\sqrt{5}m_0$, where m_0 represents the mass of the two colliding particles [65]. This calculation assumes that particles at infinity are at rest and that the collision energy derives entirely from gravitational acceleration. Importantly, this energy limit is independent of the BH's mass.

In this paper, we discuss the orbital motion of test particles moving around a regular BH within asymptotically safe gravity. The stability of circular orbits, innermost stable circular orbits (ISCOs), and the effective force acting on test particles have been discussed. We discuss the shadows of the examined BH. Furthermore, collisions of particles and the center of mass energy have been investigated.

The manuscript is structured as follows. In Sect. 2, we describe the essential characteristics of the BH spacetime under investigation. Section 3 explores the trajectory of test particles in the vicinity of a normal black hole within the framework of asymptotically safe gravity. The stability of equatorial circular orbits has been analyzed using effective potentials, innermost stable circular orbits (ISCOs), and the effective force acting on particles. The epicyclic oscillations and perturbed circular orbits are considered in Sect. 4 and constraints on the mass of regular black holes are obtained in the framework of asymptotically safe gravity in Sect. 6. Section 7 deals with the collision of particles and the energy of the center of mass. The next section describes shadows of regular BH within asymptotically safe gravity. We examine shadow behaviors and offer predictions for η using the EHT data in Sect. 8. Section 9 contains the concluding findings. We adopt geometric units $G = c = 1$ in our calculations and adopt the space-time signature $(-+++)$. Greek indices generally range from 0 to 3. Nevertheless, for expressions of astrophysical relevance, we explicitly utilize the physical constants.

2 Regular BHs in the framework of the asymptotically safe gravity

We begin with a brief review of a non-rotating regular BH in the background of asymptotically safe gravity. Recently, Bonnano et al. [17] expanded on the concepts introduced by Markov and Mukhanov [66], examining the formation of regular BH during gravitational collapse. They address this through the following action

$$I = \frac{1}{16G_N\pi}\int (R + 2\mathcal{Y}(\epsilon)\mathrm{L})\sqrt{-g}\, d^4x, \tag{1}$$

where L denotes the matter Lagrangian, and $\mathcal{Y}(\epsilon)$ ($\mathcal{Y}(0) = 8G_N\pi$) some coupling Lagrangian. The total variation of the action (1) gives the following differential equations

$$R_{\alpha\beta} = \frac{R\, g_{\alpha\beta}}{2} = 8\pi T_{\alpha\beta}G(\epsilon) - g_{\alpha\beta}\,\Lambda(\epsilon), \tag{2}$$

where

$$T_{\alpha\beta} = (p(\epsilon) + \epsilon)u_\alpha u_\beta + p g_{\alpha\beta}, \tag{3}$$

denotes the energy-momentum tensor of the ideal fluid, while $\Lambda(\epsilon)$ and $G(\epsilon)$ represents the cosmological constant and effective gravitational constant, given by

$$\Lambda(\epsilon) = \frac{\partial \mathcal{Y}}{\partial \epsilon}\epsilon^2, \tag{4}$$

$$8\pi G(\epsilon) = \frac{\partial(\mathcal{Y}\epsilon)}{\partial\epsilon}. \tag{5}$$

A renormalization group trajectory closer to the ultraviolet fixed point of the asymptotic safety program [17] determines the behavior of $G(\epsilon)$ with regard to the function of the energy scale and was considered as:

$$G(\epsilon) = \frac{G_N}{1 + \eta\epsilon}, \tag{6}$$

where G_N is the gravitational constant, while the parameter η is the scale parameter. Some observations from [67,68] can be used to constrain the unknown value of the scale parameter η. The following metric for static outside space-time was generated by the authors [17] as a result of the gravitational collapse of dust ($p = 0$) as:

$$\mathrm{d}s^2 = -f(r)\mathrm{d}t^2 + f^{-1}(r)\mathrm{d}r^2 + r^2(\mathrm{d}\theta^2 + \sin^2\theta\mathrm{d}\phi^2), \tag{7}$$

where the unknown function $f(r)$ reads

$$f(r) = 1 - \frac{r^2}{3\eta}\ln\left(\frac{6M\eta}{r^3} + 1\right), \tag{8}$$

where M is the gravitational mass. For vanishing $\eta = 0$, the metric (7) leads to the Schwarzshild metric. The position of the horizon is calculated by solving the equation $f(r) = 0$, which can give interesting results. For any specified value of M, critical values exist given by

$$\eta_{cr} = \frac{2}{3}(3 + 2y)y^2M^2, \tag{9}$$

and

$$r_h^{ext} = -2My, \quad y = W_0(x) = W_0\left(-\frac{3}{2e^{\frac{3}{2}}}\right), \tag{10}$$

where $W_0(x)$ defines the Lambert function and the numerical values are provided as:

$$\eta_{cr} = 0.4565M^2, \quad r_{\mathrm{hoz}}^{ext} = 1.2516M. \tag{11}$$

There are the following situations

- For $\eta \in (0, \eta_{cr})$, there exist two roots of $f(r)$ that correspond to the inner horizon ($r_{\mathrm{hor}} \in (0, r_{\mathrm{hoz}}^{ext})$) and the outer horizon ($r_{\mathrm{hor}} \in (r_{\mathrm{hoz}}^{ext}, 2M)$). However, for small values of η, the outer horizon can be approximated as

$$r_{\mathrm{hoz}} = 2M - \frac{3\eta}{4M} - \frac{15\eta^2}{32M^3} + O(\eta^3). \tag{12}$$

- For $\eta = \eta_{cr}$, the outer and inner event horizons merge into a single horizon at $r_{\mathrm{hoz}} = r_{\mathrm{ext}}$, resulting in an extremal BH solution.
- For $\eta > \eta_{\mathrm{cr}}$, a horizonless configuration arises. For η approaches 0, the Schwarzschild solution can be obtained.

3 Motion of particles around regular BHs within asymptotically safe gravity

Here we examine the motion of test particles relative to a regular BH against the context of asymptotically safe gravity, and the following Hamiltonian describes the motion of a neutral particle as:

$$H = \frac{1}{2}g^{\alpha\beta}P_\alpha P_\beta + \frac{1}{2}m^2, \tag{13}$$

where m represents the mass of the particle, $P^\alpha = mU^\alpha$ signifies the four-momentum, $U^\alpha = dx^\alpha/d\tau$ indicates the four-velocity, and τ denotes the proper time of the test particle. The Hamiltonian equations of motion are expressed as:

$$\frac{dx^\alpha}{d\zeta} \equiv mU^\alpha = \frac{\partial H}{\partial P_\alpha}, \quad \frac{dP_\alpha}{d\zeta} = -\frac{\partial H}{\partial x^\alpha}, \tag{14}$$

where $\zeta = \tau/m$ represents the affine parameter. Owing to the symmetries of the black hole geometry, two constants of motion are present: a specific energy E and specific angular momentum L, which both are defined as follows

$$\frac{P_t}{m} = -\left(1 - \frac{r^2}{3\eta}\ln\left(\frac{6M\eta}{r^3}+1\right)\right)\frac{\mathrm{d}t}{\mathrm{d}\tau} = -\mathcal{E}, \tag{15}$$

$$\frac{P_\phi}{m} = r^2\sin^2\theta\,\frac{\mathrm{d}\phi}{\mathrm{d}\tau} = \mathcal{L}, \tag{16}$$

where $\mathcal{E} = E/m$ and $\mathcal{L} = L/m$ denote a particular energy and a specific angular momentum, respectively. The temporal U^t, azimuthal U^ϕ and radial U^r components of the four-velocity U^α adhere to the following equations as:

$$\dot{t} = \frac{\mathcal{E}}{1 - \frac{r^2}{3}\eta\ln\left(\frac{6M\eta}{r^3}+1\right)}, \tag{17}$$

$$\dot{\phi} = \frac{\mathcal{L}}{r^2\sin^2\theta}, \tag{18}$$

$$\dot{r}^2 + \left(\delta + \frac{L^2}{r^2\sin^2\theta}\right)f(r) = \mathcal{E}^2, \tag{19}$$

where $\delta = 1$ for time-like particles and $\delta = 0$ for null particles. The dot represents the derivative for the appropriate time τ. Our effort will concentrate exclusively on time-like particles. The Hamiltonian (13) for a conventional black hole (7) under the framework of asymptotically safe gravity is expressed as

$$H = \frac{1}{2}\left(1 - \frac{r^2}{3\eta}\ln\left(\frac{6M\eta}{r^3}+1\right)\right)P_r^2 + \frac{1}{2r^2}P_\theta^2 + \frac{1}{2}\frac{m^2}{\left(1 - \frac{r^2}{3\eta}\ln\left(\frac{6M\eta}{r^3}+1\right)\right)}\left[V_{\mathrm{eff}}(r,\theta) - \mathcal{E}^2\right], \tag{20}$$

where the effective potential $V_{eff}(r,\theta)$ can be written as

$$V_{eff}(r,\theta) = \left(1 + \frac{\mathcal{L}^2\csc^2\theta}{r^2}\right)\left(1 - \frac{r^2}{3\eta}\ln\left(\frac{6M\eta}{r^3}+1\right)\right). \tag{21}$$

For $\eta = 0$, the effective potential (21) leads to the Schwarzschild case.

3.1 Equatorial circular orbits

The effective potential $V_{eff}(r,\theta)$ is crucial for understanding the dynamics of the test particles. It provides a means to describe the motion of particles independently of explicit equations of motion. The stable and unstable circular orbits correspond to the minimum and maximum values of V_{eff}, respectively. The behavior of the effective potential for the equatorial orbits is shown in Fig. 1. In the first row and first column, the behavior of effective potential is shown for different values of the BH parameter η, while the behavior of effective potential for different values of angular momentum $\mathcal{L}$ is shown for $\eta < \eta_{cr}$ and $\eta = \eta_{cr}$. When $\eta < \eta_{cr}$, the effective potential does not increase much as we increase the values of angular momentum. It is interesting to note that both the BH parameter η and the particle's angular momentum $\mathcal{L}$ behave similarly on effective potential. The effective potential increases with increasing either the BH parameter η or the angular momentum of the particle $\mathcal{L}$. When the particles move close to the event horizon of the BH, the circular orbits are stable, and stability decreases as the particles move away from the BH. The circular orbits in an equatorial plane $\theta = \pi/2$ can be found by the simultaneous conditions

$$V_{\mathrm{eff}}(r) = \mathcal{E}^2, \quad \frac{\mathrm{d}V_{\mathrm{eff}}(r)}{\mathrm{d}r} = 0. \tag{22}$$

To resolve Eq. (22), we derive the circular orbits within the context of a non-rotating regular black hole with asymptotically safe gravity (7), expressed as

$$\mathcal{L} = \frac{r^2\sqrt{\frac{9M}{6\eta M+r^3} - \frac{\ln\left(\frac{6\eta M}{r^3}+1\right)}{\eta}}}{\sqrt{3 - \frac{9Mr^2}{6\eta M+r^3}}}, \tag{23}$$

and

$$\mathcal{E} = \frac{3\eta - r^2\ln\left(\frac{6\eta M}{r^3}+1\right)}{3\eta\sqrt{1 - \frac{3Mr^2}{6\eta M+r^3}}}. \tag{24}$$

For $\eta = 0$, the Eqs. (23) and (24) reduces to the case of Schwarzschild BH. Figure 2 describes the behavior of the energy as a function of r for varying values of the BH parameter η. It is shown that when the value of the BH parameter η is small, the particles have a large energy; however, the energy behavior decreases for large values of η. The behavior of the angular momentum increases monotonically as the radial distance r increases. Figure 2 describes the behavior of the energy as a function of r for varying values of the BH parameter η. It is shown that when the value of the BH parameter η is small, the particles have a large angular momentum, while the particles have a small angular momentum for increasing values of the BH parameter η. However, the behavior of the angular momentum increases monotonically as the radial distance r increases.

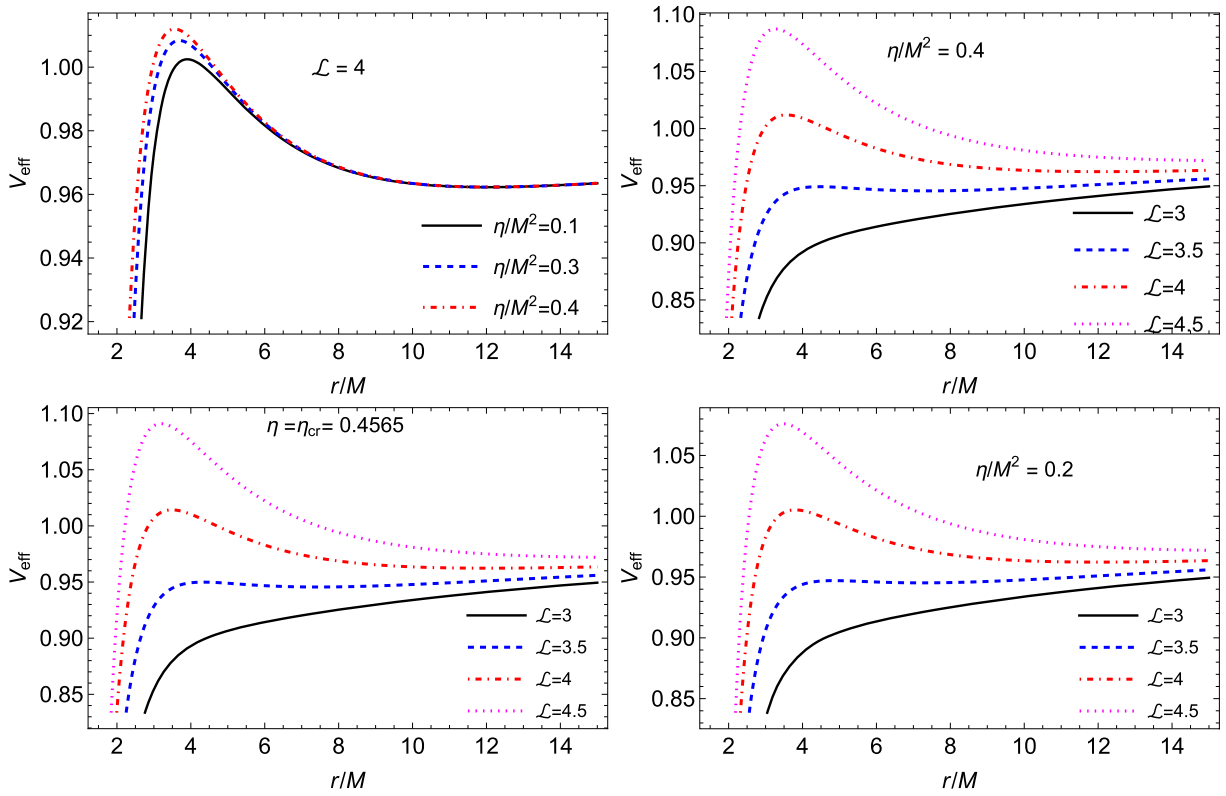

Fig. 1 Behaviour of the effective potential for the test particles in the background of regular BH in asymptotically safe gravity

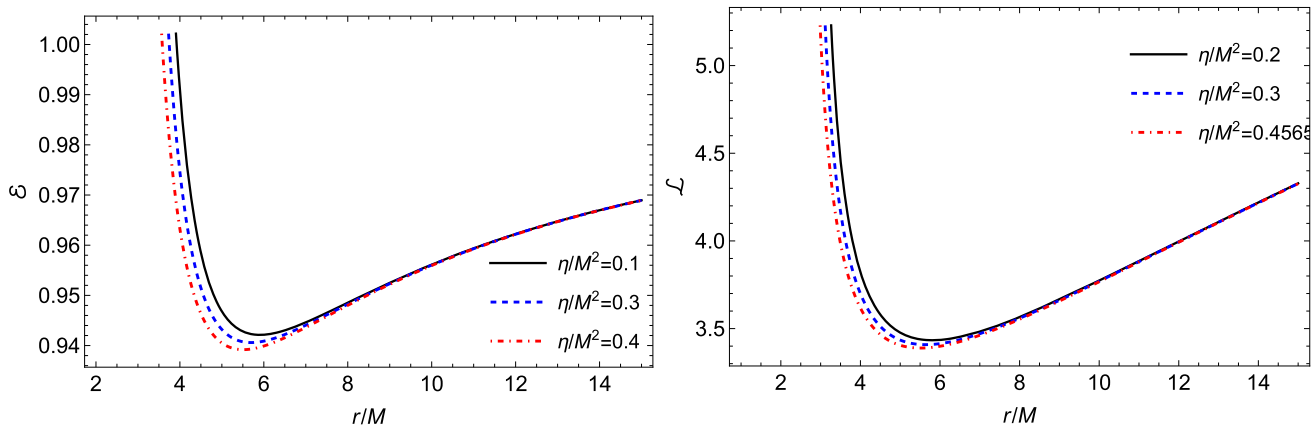

Fig. 2 Behavior of energy (left) and angular momentum (right) of the circular orbits as a function of r in the background of regular BH in asymptotically safe gravity

3.2 Regular BHs in asymptotically safe gravity and innermost stable circular orbits

The extremum of the effective potential signifies the positions of stable and unstable circular orbits, respectively. In Newtonian theory, the effective potential exhibits a minimum radius that corresponds to the Innermost Stable Circular Orbit (ISCO) for any specified angular momentum. Nevertheless, as elements such as the particle's rotational momentum and other attributes affect the effective potential, its structure becomes more intricate, resulting in alterations to the positions of these circular orbits. Thus, in General Relativity, the effective potential for particles nearing a Schwarzschild black hole can display two extreme states for a specified angular momentum. An accurate calculation of the angular momentum is essential for discussing the position of the ISCO in the current analysis. The locations of ISCOs can be determined according to the specified requirements by taking following relations:

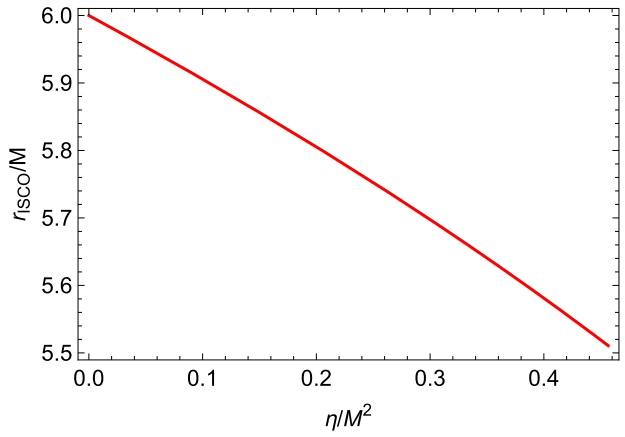

Fig. 3 Behaviour of the ISCOs of particles, as a function of BH parameter η/M^2 in the background of regular BH in asymptotically safe gravity

$$V_{\rm eff}(r) = \mathcal{E}^2, \quad \frac{{\rm d}V_{\rm eff}(r)}{{\rm d}\,r} = 0, \quad \frac{{\rm d}^2 V_{\rm eff}(r)}{{\rm d}\,r^2} = 0. \tag{25}$$

The radii of ISCOs for the present non-rotating regular black hole in the context of asymptotically safe gravity can be determined using the last expression of Eq. (25). The behavior of equatorial ISCOs surrounding a non-rotating regular black hole within the context of asymptotically safe gravity is illustrated in Fig. 3. The behavior is depicted as a function of the BH parameter η. The radii of the ISCOs decrease as the BH parameter η increases. The ISCOs surrounding non-rotating regular black holes in the context of asymptotically safe gravity are less than those associated with the Schwarzschild black hole.

3.3 Effective force

The net force exerted on a particle indicates its velocity, which indicates whether it is being dragged into the black hole or going away from it. We examine the particle's motion in the context of a non-rotating regular BH within asymptotically safe gravity, where both attractive and repulsive gravitational forces can occur. Using Eq. (22), we determine the effective force acting on the particles, which is given by

$$F = -\frac{1}{2}\frac{dV_{eff}}{dr}, \tag{26}$$

for the current BH solution, it is calculated as:

$$F = \frac{3\eta\mathcal{L}^2\left(6\eta + (r-3)r^2\right) - 9\eta r^4 + F_1}{2\sqrt{3}\eta r^2\left(6\eta + r^3\right)F_2}, \tag{27}$$

where

$$F_1 = r^4\left(6\eta + r^3\right)\ln\left(\frac{6\eta}{r^3} + 1\right),$$

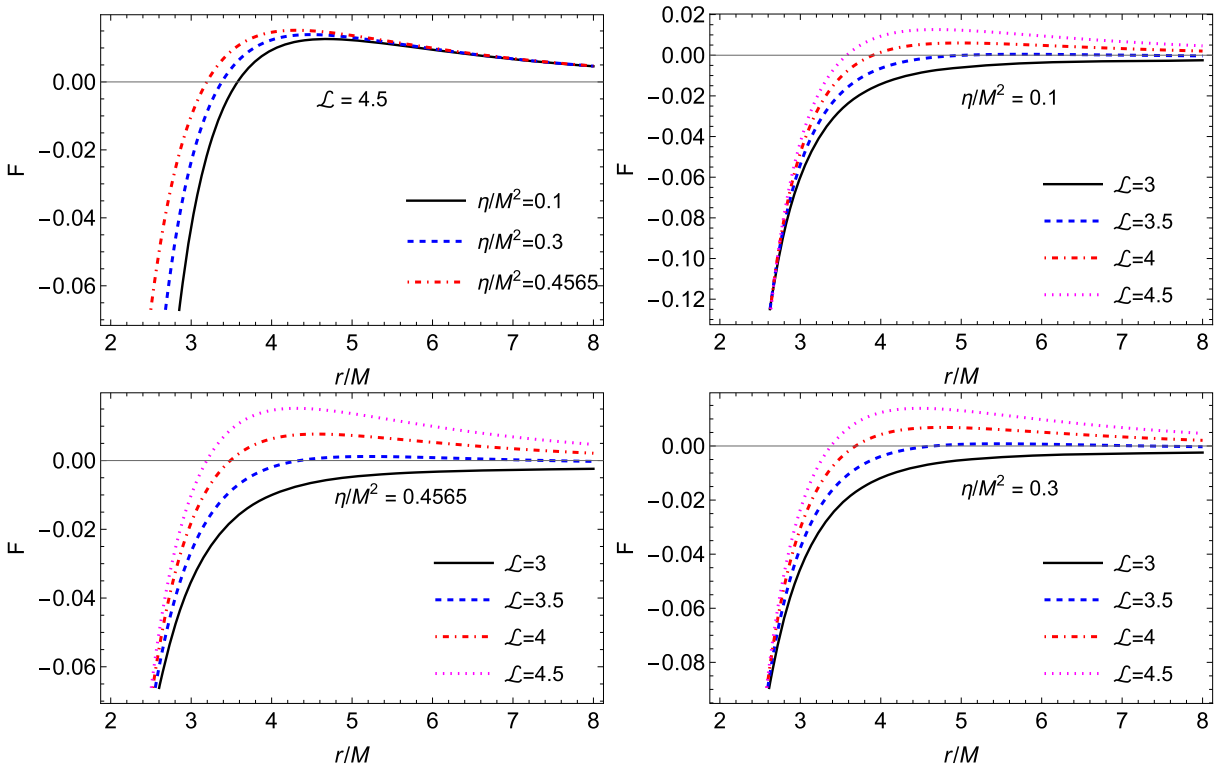

Fig. 4 Behaviour of effective force acting on particles in the background of regular BH in asymptotically safe gravity

$$F_2 = \sqrt{\frac{\left(\mathcal{L}^2 + r^2\right)\left(3\eta - r^2 \ln\left(\frac{6\eta}{r^3}+1\right)\right)}{\eta}}.$$

The behavior of the effective force around the non-rotating regular BH in the background of asymptotically safe gravity is shown in Fig. 4, as a function of r, for the parameter of varying values of BH η and the angular momentum. It is noted that the effective force acting on the particles has the same behavior for both the parameters η and the angular momentum. The effective force is small when the parameter η or the angular momentum $\mathcal{L}$ has small values, however, the effective force increases when the parameter η or angular momentum $\mathcal{L}$ increases. When we fix the angular momentum and vary the BH parameter η, the effective force radial profiles coincide as the radial distance r increases. However, for varying values of angular momentum, different radial profiles of effective force can be observed as the radial distance r increases.

4 Epicyclic oscillations and perturbed circular orbits

To examine the oscillatory motion of neutral particles, we perturb the equations of motion near ISCOs. A test particle displaced marginally from the equilibrium point of a stable circular orbit in the equatorial plane will experience epicyclic motion, defined by linear harmonic oscillations.

4.1 Frequencies measured by local observer

The frequencies of harmonic oscillatory motion measured by the local observer are given by

$$\omega_r^2 = \frac{-1}{2}\frac{\partial^2 V_{\text{eff}}(r,\theta)}{\partial r^2}, \tag{28}$$

$$\omega_\theta^2 = \frac{1}{2}\frac{g_{rr}(r,\theta)}{r^2}\frac{\partial^2 V_{\text{eff}}(r,\theta)}{\partial \theta^2}, \tag{29}$$

$$\omega_\phi = \frac{\mathrm{d}\phi}{\mathrm{d}\tau}. \tag{30}$$

The radial (ω_r), latitudinal (ω_θ), and orbital/axial (ω_ϕ) frequencies of the neutral test particle around non-rotating regular BHs within asymptotically safe gravity takes the form

$$\omega_r^2 = \frac{1}{\mathcal{Z}_1}\left(\mathcal{Z}_2\mathcal{Z}_3\left(L^2 + r^2\right) + \mathcal{Z}_4\right), \tag{31}$$

$$\omega_\theta^2 = \omega_\phi^2 = \frac{9\eta M - \left(6\eta M + r^3\right)\ln\left(\frac{6\eta M}{r^3}+1\right)}{3\eta\left(6\eta M - 3Mr^2 + r^3\right)}, \tag{32}$$

where

$$\mathcal{Z}_1 = 2\sqrt{3}\eta^2 r^3\left(6\eta M + r^3\right)^2$$

$$\left(\frac{\left(L^2 + r^2\right)\left(3\eta - r^2\log\left(\frac{6\eta M}{r^3}+1\right)\right)}{\eta}\right)^{3/2},$$

$$\mathcal{Z}_2 = r^4\left(6\eta M + r^3\right)^2\log\left(\frac{6\eta M}{r^3}+1\right) - 9\eta\left(L^2\left(-6\eta M^2\left(r^2 - 6\eta\right) - 4M\left(r^5 - 3\eta r^3\right) + r^6\right) + 18\eta M^2 r^4\right),$$

$$\mathcal{Z}_3 = \left(3\eta - r^2\log\left(\frac{6\eta M}{r^3}+1\right)\right),$$

$$\mathcal{Z}_4 = \left(3\eta L^2\left(6\eta M - 3Mr^2 + r^3\right) - 9\eta M r^4 + r^4\left(6\eta M + r^3\right)\log\left(\frac{6\eta M}{r^3}+1\right)\right)^2.$$

For vanishing black hole parameters $\eta = 0$, Eqs. (31)–(32) simplify to the radial, latitudinal, and axial frequencies of test particles in the vicinity of a Schwarzschild black hole. Equations (31) and (32) clearly indicate $\omega_\theta = \omega_\phi$.

4.2 Frequencies measured by distant observer

The locally defined angular frequencies ω_β are delineated in Eqs. ((31)–(32)). Conversely, the angular frequencies observed by a stationary distant observer (Ω) are expressed as:

$$\Omega_\beta = \omega_\beta\frac{\mathrm{d}\tau}{\mathrm{d}t}, \tag{33}$$

where $\mathrm{d}\tau/\mathrm{d}t$ is the redshift coefficient, given by

$$\frac{\mathrm{d}t}{\mathrm{d}\tau} = -\frac{\mathcal{E}}{g_{tt}}. \tag{34}$$

When a distant observer measures the frequencies of minor harmonic oscillations in physical units, the frequencies of neutral particles, as ascertained by these observers, assume the following form

$$\nu_i = \frac{1}{2\pi}\frac{c^3}{GM}\Omega_i\,[\text{Hz}], \tag{35}$$

where $i \in \{r, \theta, \phi\}$; Ω_r, Ω_θ, and Ω_ϕ denotes the dimensionless radial, latitudinal, and axial angular frequencies measured by a distant observer, given by

$$\Omega_r^2 = \frac{27\eta\left(12\eta + (r-4)r^2\right)}{3\eta\left(6\eta + r^3\right)^2} + \frac{\left(-144\eta^2 - 4r^6 + 15r^5 - 48\eta r^3 + 36\eta r^2\right)\log\left(\frac{6\eta}{r^3}+1\right)}{3\eta\left(6\eta + r^3\right)^2}, \tag{36}$$

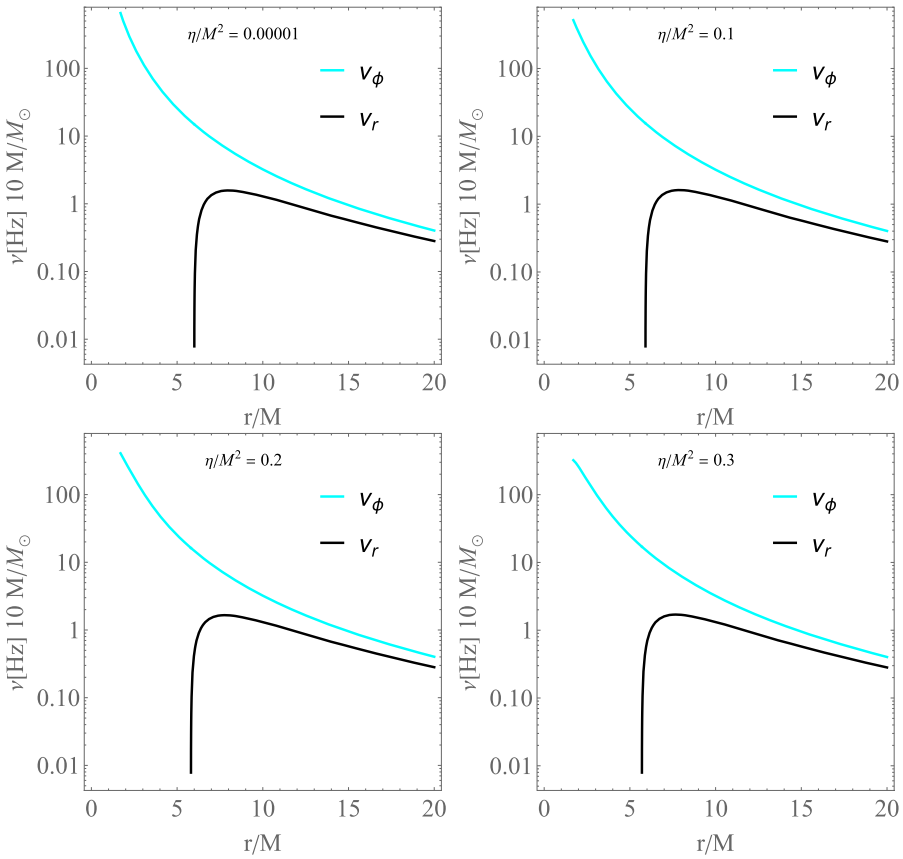

Fig. 5 Frequencies of particles moving around regular BHs within asymptotically safe gravity, for different values of BH parameters η

$$\Omega_\theta^2 = \Omega_\phi^2 = \frac{3}{6\eta + r^3} - \frac{\log\left(\frac{6\eta}{r^3}+1\right)}{3\eta}, \tag{37}$$

The radial profiles of frequencies ν_j, detected by a distant observer, for small harmonic oscillations of neutral particles around non-rotating regular BHs within asymptotically safe gravity for different values of BH parameter η are shown in Fig. 5. The radial profiles for the orbital frequency (Ω_ϕ) and the latitudinal frequency (Ω_θ) coincide, which is a typical behavior for the frequencies of particles around non-rotating BHs. The BH parameter η contributes to the shift in the fundamental frequencies of the test particles close to the BH horizon. The particles around Schwarzschild BH have higher frequencies as compared to those particles traveling around regular BH within asymptotically safe gravity.

4.3 Periastron precession

This section addresses the periastron frequency of a neutral test particle orbiting a non-rotating regular black hole within the framework of asymptotically safe gravity, considering the limit of a little perturbation relative to the equatorial plane at $\pi/2$. To compute the Periastron precession, we suppose that the particle is minimally disturbed from its stable location, leading to oscillations around that point with a radial frequency Ω_r. The periastron frequency Ω_P is defined as the difference between the orbital frequency Ω_ϕ and the radial frequency Ω_r, expressed by the relation

$$\Omega_P = \Omega_\phi - \Omega_r, \tag{38}$$

$$\Omega_P = \sqrt{\frac{3M}{6\eta M + r^3} - \frac{\ln\left(\frac{6\eta M}{r^3}+1\right)}{3\eta}} - \frac{\sqrt{\frac{P_1}{P_2}}}{\sqrt{3}}, \tag{39}$$

where

$$P_1 = \left(36\eta M^2\left(r^2-4\eta\right) + 3M\left(5r^5 - 16\eta r^3\right) - 4r^6\right)\ln\left(\frac{6\eta M}{r^3}+1\right) + 27\eta M \times \left(r^3 - 4M\left(r^2-3\eta\right)\right),$$

$$P_2 = \eta\left(6\eta M + r^3\right)^2.$$

The graphical behavior of periastron frequency for particles orbiting a non-rotating regular black hole within the framework of asymptotically safe gravity is illustrated in Fig. 6. The frequency of the periastron is shown to decrease with an increase in the parameter η and likewise decrease with increasing radial distance r.

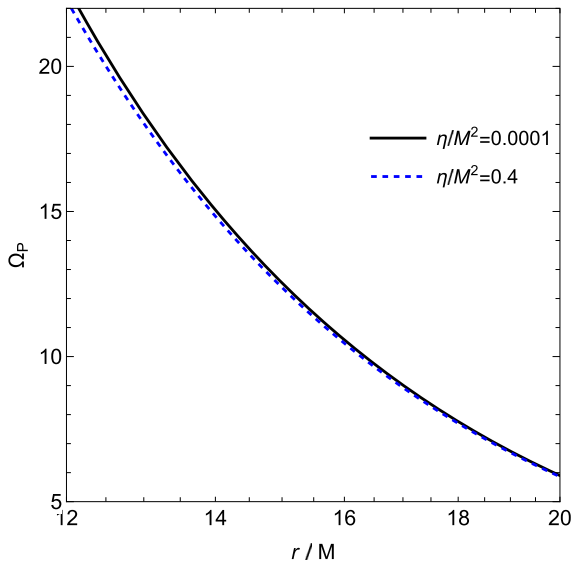

Fig. 6 Periastron frequency of particles in the background of regular BHs within asymptotically safe gravity, for varying values of BH parameter η

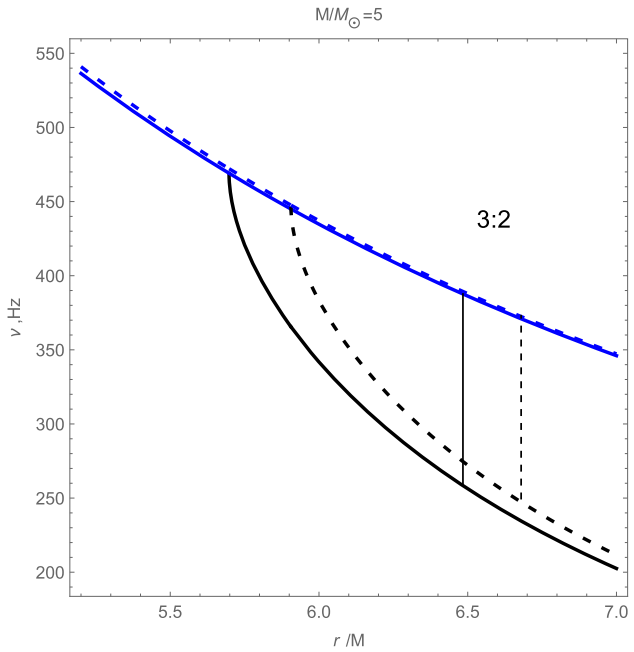

Fig. 7 The radial profile of the upper (ν_U , blue) and lower (ν_L, black) frequencies is presented for the RP model. The panel displays results for two distinct values of η/M^2 (solid lines for $\eta/M^2 = 0.3$, while dashed lines for $\eta/M^2 = 0.1$). Furthermore, $r_{3:2}$ resonance radii are also displayed by solid and dashed vertical lines

5 Relativistic precession model

The relativistic precession (RP) model [69,70] is one of the most widely used frameworks for explaining quasi-periodic oscillations (QPOs) observed in X-ray binaries. This model attributes QPO frequencies to the fundamental oscillatory motion of matter in the strong gravitational field of a compact object, such as a black hole. Specifically, it links observed QPO frequencies to the orbital, radial, and vertical epicyclic motion of matter within an accretion disk.

In the RP model, the three key frequencies are:

- **Orbital frequency** (ν_ϕ): The Keplerian frequency at which a particle orbits the compact object.
- **Radial epicyclic frequency** (ν_r): The frequency of small radial perturbations around the circular orbit.
- **Vertical epicyclic frequency** (ν_θ): The frequency of small vertical perturbations around the orbital plane.

The twin-peak QPOs observed in many X-ray binaries are interpreted within the RP model as follows:

$$\nu_U = \nu_\phi, \quad \text{(Upper QPO frequency)} \tag{40}$$

$$\nu_L = \nu_\phi - \nu_r. \quad \text{(Lower QPO frequency)} \tag{41}$$

This model naturally explains the observed 3:2 frequency ratio in high-frequency QPOs (HFQPOs) as a resonance condition between these fundamental oscillatory modes [71,72].

5.1 Application to the asymptotically safe gravity

In our study, we apply the RP model to the asymptotically safe gravity, where the presence of the parameter η modifies the orbital and epicyclic frequencies. The effect of η on QPO frequencies is crucial for understanding observational constraints on this parameter.

Figure 7 illustrates the variation of the upper and lower QPO frequencies as functions of r/M for different values of η. Notably, the 3:2 resonance occurs at different radii depending on η, which implies that the parameter influences the possible locations where QPOs can be detected.

Figure 8 shows the relationship between the upper and lower QPO frequencies for various values of η. The modification in this relationship compared to the standard RP model suggests that future X-ray observations could potentially constrain η by identifying deviations from the expected Schwarzschild predictions.

The $\nu_U/\nu_L \approx 3/2$ condition allows us to determine r as a function of the black hole mass. Figure 9 illustrates the relationship between the lower frequency and r, with results derived from this condition, alongside selected datasets. As mentioned, the spacetime parameter must lie within its maximum and minimum values, which are indicated by the shaded region. This implies that the spacetime model can only account for the data within this shaded area. From Fig. 9, only two data points are available; however, since GRS

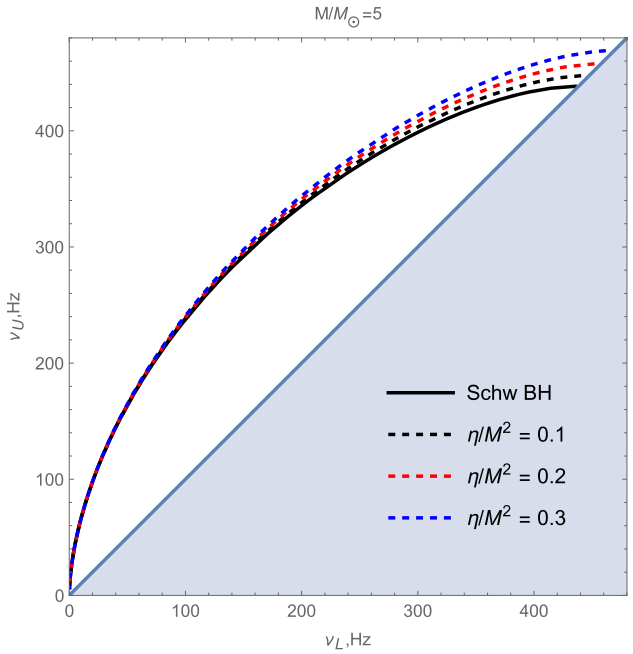

Fig. 8 The relationships between the frequencies of the upper and lower peaks of the twin-peak QPOs in the RP model are investigated around a BH of asymptotical safe gravity with a mass of $M = 5M_{\odot}$

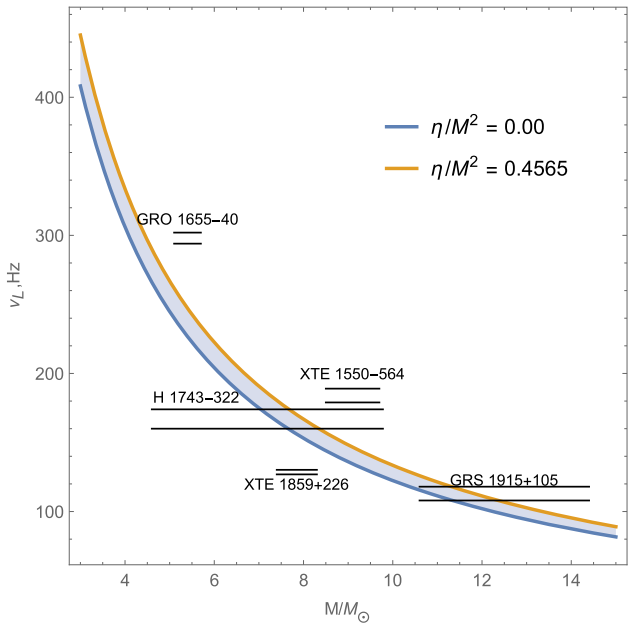

Fig. 9 The lower frequency as a function of the black hole mass (measured in solar mass units)

Table 1 The mass, upper and lower frequencies of QPOs from the X-ray binaries selected for analysis

	H1743-322
$M(M_{\odot})$	$\leq$9.78 [80]
ν_{up}(Hz)	240 ± 3 [80]
ν_{low}(Hz)	165^{+9}_{-5} [80]

Table 2 The Gaussian prior of the BHs within asymptotically safe gravity derived from QPOs for the selected X-ray sources

Parameters	H1743-322
$M(M_{\odot})$	8.2 ± 0.25
r/M	6.5 ± 0.2
η/M^2	0.25 ± 0.012

Table 3 The best-fit parameter values resembling those of BHs within asymptotically safe gravity, deduced from the QPOs for the chosen X-ray sources

Parameters	H1743-322
$M(M_{\odot})$	8.16 ± 0.17
r/M	$6.44^{+0.08}_{-0.07}$
η/M^2	0.25 ± 0.02

1915+105 corresponds to a rotating case, it cannot be used in this analysis. Additionally, the figure provides prior values (2) for the Markov Chain Monte Carlo (MCMC) analysis.

6 Constraints on the mass of a asymptotically safe black hole

This section examines X-ray binary systems to provide limitations on the parameters of our considered black hole model. This entails analyzing QPOs data from these systems, focusing on source H1743-322. We will ultimately present the optimal parameter values obtained via Markov Chain Monte Carlo (MCMC) research. The MCMC analysis was performed with the Python package 'emcee' [73], with the objective of establishing constraints on the black hole parameters derived from the relativistic precession (RP) model. The posterior distribution is delineated as specified in [74]:

$$\mathcal{P}(\Theta|D, M) = \frac{P(D|\Theta, M)\pi(\Theta|M)}{P(D|M)},$$

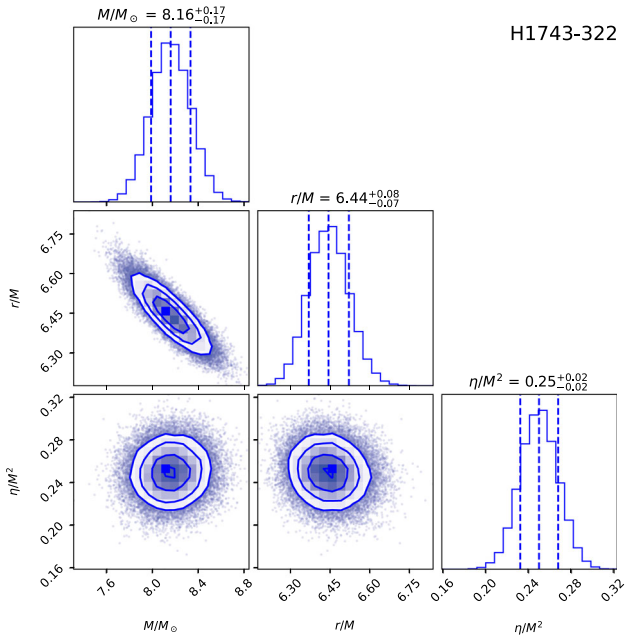

Fig. 10 Constraints on BHs mass within asymptotically safe gravity, the η parameter in the microquasar H1743-322 using MCMC code

where: - $\pi(\Theta)$ represents the prior distribution, - $P(D|\Theta, M)$ is the likelihood. The priors are Gaussian within set boundaries:

$$\pi(\Theta_i) \sim \exp\left(-\frac{1}{2\sigma_i^2}(\Theta_i - \Theta_0)^2\right),$$

subject to $\Theta_{\text{low},i} < \Theta_i < \Theta_{\text{high},i}$ for the parameters $\Theta_i = [M, r/M, \eta/M^2]$, where σ_i are their standard deviations. We use η/M^2 and $r = r_{3:2}/M$ to denote the normalized radial location of the 3:2 resonance. Table 2 lists the prior values for the parameters of the safe gravity [75–79].

Incorporating the upper and lower frequency data obtained in Fig. (8) by Eq. (7), our MCMC analysis utilizes two distinct datasets. Central to this analysis is the likelihood function, $\mathcal{L}$, which is formulated as:

$$\log \mathcal{L} = \log \mathcal{L}_{\text{up}} + \log \mathcal{L}_{\text{low}}.$$

This means that the logarithm of the likelihood function is expressed as the sum of the logarithms of the likelihoods for the upper and lower frequency datasets. Specifically, $\log \mathcal{L}_{\text{up}}$ represents the likelihood associated with the upper frequency data and is given by:

$$\log \mathcal{L}_{\text{up}} = -\frac{1}{2}\sum_i \left(\frac{(\nu^i_{\text{up, obs}} - \nu^i_{\text{up, th}})^2}{(\sigma^i_{\text{up, obs}})^2}\right).$$

Similarly, $\log \mathcal{L}_{\text{low}}$ denotes the likelihood related to the lower frequency data, formulated as:

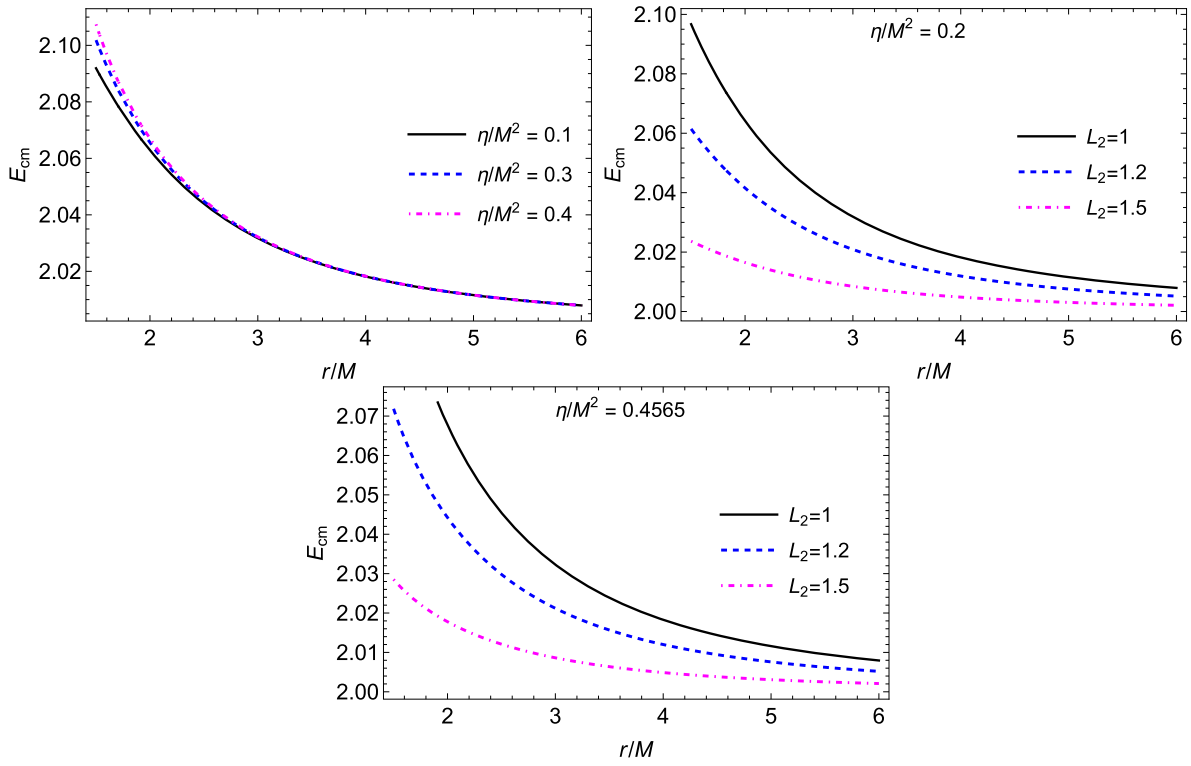

Fig. 11 Behaviour of the center of mass energy as a function of radial distance r in the background of regular BH in asymptotically safe gravity

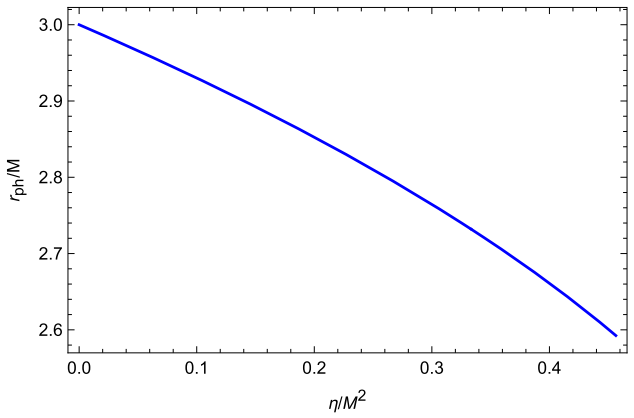

Fig. 12 Dependence of the photon sphere radius on the parameter η/M^2

$$\log \mathcal{L}_{\text{low}} = -\frac{1}{2}\sum_i \left(\frac{(\nu^i_{\text{low, obs}} - \nu^i_{\text{low, th}})^2}{(\sigma^i_{\text{low, obs}})^2} \right)$$

Here, i indexes the upper and lower frequencies measured. The upper and lower frequencies observed are denoted $\nu^i_{\text{up, obs}}$ and $\nu^i_{\text{low, obs}}$, while $\nu^i_{\text{up, th}}$ and $\nu^i_{\text{low, th}}$ refer to their theoretical counterparts. The terms σ^i_{up} and σ^i_{low} indicate the statistical uncertainties of these values (Table 1).

7 Collisions of particles

This section examines the collision of two neutral test particles possessing identical rest mass μ, differing four-velocities, and moving inside the same plane. The center of mass energy of these particles is determined as (Tables 2, 3; Fig. 10):

$$\frac{E_{cm}}{\sqrt{2}m_0} = \sqrt{1 - g_{\alpha\beta}u^\alpha u^\beta}, \tag{42}$$

where

$$u^\alpha_i = \left(\frac{\mathcal{E}_i}{\left(1 - \frac{r^2}{\eta}\ln\left(\frac{6M\eta}{r^3}+1\right)\right)}, -Y_i, 0, \frac{\mathcal{L}_i}{r^2} \right), \tag{43}$$

and

$$Y_i = \sqrt{\mathcal{E}_i^2 - \left(1+\frac{\mathcal{L}^2}{r^2}\right)\left(1 - \frac{r^2}{\eta}\ln\left(\frac{6M\eta}{r^3}+1\right)\right)}, \tag{44}$$

where $\mathcal{E}_i\,(i=1,2)$ and $\mathcal{L}_i\,(i=1,2)$ represent the energy and angular momentum of the respective particles. The energy of the center of mass is contingent upon the interacting particles and the gravitational field surrounding the astrophysical entity. The total energy of two interacting particles is determined by summing their rest masses and kinetic energies. For a non-rotating regular black hole in the context of asymptotically safe gravity, the center of mass energy is expressed as:

$$\frac{E_{cm}}{\sqrt{2}m_0} = \sqrt{1 + \frac{\mathcal{E}_1\mathcal{E}_2}{f(r)} - \frac{Y_1Y_2}{f(r)} - \frac{\mathcal{L}_1\mathcal{L}_2}{r^2}}, \tag{45}$$

and further it is defined as:

$$\frac{E_{cm}}{\sqrt{2}m_0} = \sqrt{\frac{\eta r^2(\chi_1\chi_2 - 3\mathcal{E}_1\mathcal{E}_2 - 3) + \chi_3}{r^4\ln\left(\frac{6\eta M}{r^3}+1\right) - 3\eta r^2}}, \tag{46}$$

where the functions χ_1 and χ_2 take the following form

$$\chi_1 = \sqrt{3\mathcal{E}_1^2 + \frac{(\mathcal{L}_1^2 + r^2)\ln\left(\frac{6\eta M}{r^3}+1\right)}{\eta} - \frac{3\mathcal{L}_1^2}{r^2} - 3},$$

$$\chi_2 = \sqrt{3\mathcal{E}_2^2 + \frac{(\mathcal{L}_2^2 + r^2)\ln\left(\frac{6\eta M}{r^3}+1\right)}{\eta} - \frac{3\mathcal{L}_2^2}{r^2} - 3},$$

$$\chi_3 = 3\eta\mathcal{L}_1\mathcal{L}_2 + \left(r^4 - \mathcal{L}_1\mathcal{L}_2 r^2\right)\ln\left(\frac{6\eta M}{r^3}+1\right).$$

The center of mass energy will become infinite if one of the colliding particles possesses diverging angular momentum at the event horizon. Consequently, for finite center-of-mass energy levels, only finite angular-momentum values are permissible. Figure 11 illustrates the graphical representation of the center-of-mass energy as a function of radial distance r surrounding a non-rotating normal black hole within the context of asymptotically safe gravity. The first row and first column display the behavior of the center-of-mass energy for various values of the black hole parameter η. The center of mass energy is elevated near the event horizon of the black hole but diminishes as one distances from the black hole. For small values of the BH parameter η, the center of mass energy is low, the center of mass energy increases as we increase the value of the BH parameter η. We have also shown the behavior of the center-of-mass energy for different values of angular momentum of one of the colliding particles for three different cases, i.e. $\eta < \eta_{cr}$, $\eta = \eta_{cr}$, and. It is interesting to note that the behavior of the BH parameter η on the center of mass energy and the behavior of the angular momentum of one of the colliding particles on the center of mass energy are opposite. In contrast to the BH parameter η, the energy of the center of mass decreases as the angular momentum values increase. High energy can be produced for the case $\eta < \eta_{cr}$, as compared to the cases $\eta = \eta_{cr}$.

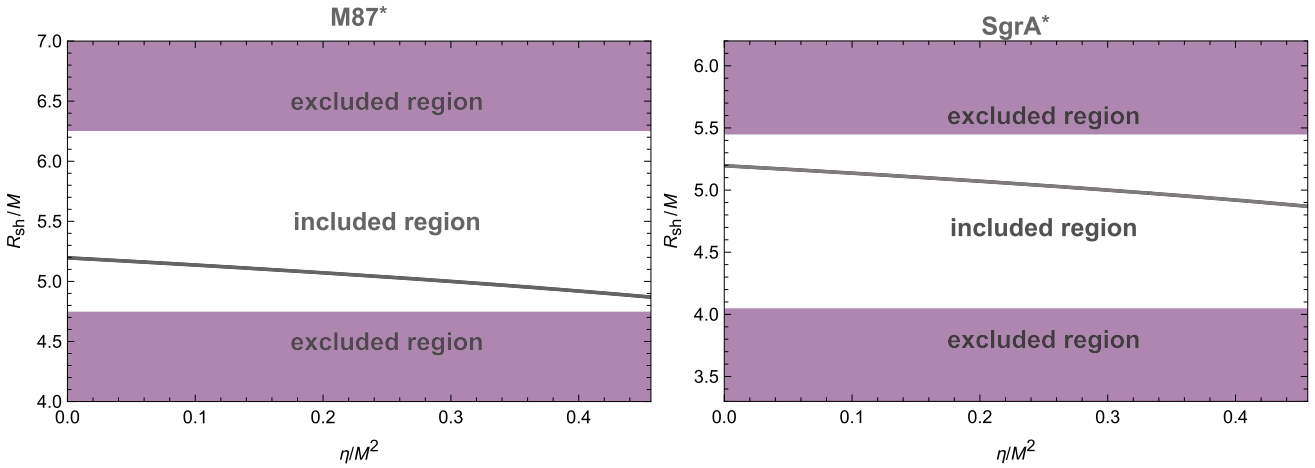

Fig. 13 The angular diameter of shadow for regular BH within the asymptotically safe gravity as a function of parameter η where angular diameter $\Omega = 42 \pm 3\,\mu$as for M87* (left panel); and for $\Omega = 48.7 \pm 7\,\mu$as for Sgr A* (right panel)

8 Black hole shadow with M87* and Sgr A*

This section examines the shadow of the regular black hole in the background of asymptotically safe gravity. A geometry-based method determines the angular radius α of the black hole's shadow [56,81]

$$\sin^2 \alpha_{sh} = \frac{h^2(r_{ph})}{h^2(r_o)}, \tag{47}$$

where

$$h^2(r_{ph}) = \frac{r_{ph}^2}{f(r_{ph})}, \quad h^2(r_o) = \frac{r_o^2}{f(r_o)}. \tag{48}$$

The position of the observer is represented by r_o, whereas the photon sphere radius r_{ph} is determined by the following equation.

$$\frac{\mathrm{d}(h^2(r))}{\mathrm{d}r}\Big|_{r=r_{ph}} = 0. \tag{49}$$

By placing the observer at quite a distance from the black hole and using Eqs. (47) and (48) we can get an approximate formula for the radius of the black hole's shadow as [56,81]

$$R_{sh} \approx r_0 \sin \alpha_{sh} = \sqrt{r_p^2 \frac{1}{f(r_p)}}. \tag{50}$$

Figure 12 shows the dependence of the photon sphere radius on the parameter η/M^2. We can see from the graph that photon sphere radius decreases as parameter η/M^2 increase. Now we consider the supermassive BHs M87 and Sgr A to be regular black holes in the background of asymptotically safe gravity. We employ observational data supplied by the EHT project for the BH shadows of the supermassive BHs M87* and Sgr A*, therefore constraining this parameter η in the background of safe gravity. The angular diameter of the shadow, the distance from the solar system, and the mass of the BH at the center of the galaxy M87 are $\Omega_{\mathrm{M87}^*} = 42 \pm 3\,\mu$as, $D = 16.8 \pm 0.8$ Mpc and $M_{\mathrm{M87}^*} = (6.5 \pm 0.7)^9\, M_\odot$ respectively [18]. Data recently acquired by the EHT project for the $\Omega_{\mathrm{Sgr\,A}^*} = 48.7 \pm 7\,\mu$as, $D = 8277 \pm 9 \pm 33$ pc and $M_{\mathrm{Sgr\,A}^*} = 4.297 \pm 0.013\mathrm{x}10^6\, M_\odot$ (VLTI) [82]. We can now derive the diameter of the shadow using the calculation $d_{\mathrm{sh}}^{\mathrm{theo}} = 2R_{\mathrm{sh}}$. The diameter of the black hole shadow image is $d_{\mathrm{sh}}^{\mathrm{M87}^*} = (11 \pm 1.5)M$ for M87* and $d_{\mathrm{sh}}^{\mathrm{Sgr\,A}^*} = (9.5 \pm 1.4)M$ for Sgr A*. Based on the data from the EHT collaboration, we derive the constraint on the parameter η for the supermassive black holes at the centers of galaxies M87* and Sgr A*. We provide our findings illustrated in Fig. 13. The image illustrates that the radius of the black hole shadow decreases as the parameter η increases. It is clear from the graph that the values $0 < \eta/M^2 < 0.4565$ are in complete agreement with the EHT observations for M87* and SgrA*. In the range $\eta/M^2 > 0.4565$, the spacetime no longer possesses horizons, indicating the presence of a horizonless compact object characterized by two photon rings [83].

9 Conclusions

We have explored the circular motion of neutral test particles around non-rotating regular BH within asymptotically safe gravity and investigated the effects of parameters of the BH on the particle's motion. We have discussed the stability of equatorial circular orbits using the effective potential approach. The behavior of the effective potential is shown for different values of the BH parameter η, and for different val-

ues of the angular momentum $\mathcal{L}$ for $\eta < \eta_{cr}$ and $\eta = \eta_{cr}$. The unstable and stable circular orbits, respectively, correspond to the maximum and minimum effective potentials. When $\eta < \eta_{cr}$, the effective potential does not increase much as we increase the values of angular momentum. It is interesting to note that both the BH parameter η and the particle's angular momentum $\mathcal{L}$ behave similarly on effective potential. The effective potential increases with increasing either the BH parameter η or the angular momentum of the particle $\mathcal{L}$. It is noted that when the particles travel close to the event horizon of BH, the circular orbits are stable, and stability decreases as we particles move away from the BH.

We have obtained the analytical expressions for energy and angular momentum of equatorial circular orbits around non-rotating regular BH within asymptotically safe gravity, as a function of BH parameters. It is noted that when the value of the BH parameter η is small, the particles have a high energy; however, the energy decreases for large values of η. Furthermore, the energy increases monotonically as the radial distance r increases. We have shown the behavior of the angular momentum as a function of r for varying values of the BH parameter η. It is shown that when the value of the BH parameter η is small, the particles have a large angular momentum, while the particles have a small angular momentum for increasing values of the BH parameter η. However, the angular momentum increases monotonically as the radial distance r increases.

The position of ISCOs plays an important role in the motion of particles around BHs. We have discussed the behavior of equatorial ISCOs around non-rotating regular BH in the background of asymptotically safe gravity, as a function of the BH parameter η. The radii of the ISCOs are observed to decrease with increasing BH parameter η. The ISCOs around non-rotating regular BH in the background of asymptotically safe gravity are smaller than in the case of the Schwarzschild BH. We have also examined the effective force around non-rotating regular BH in the background of asymptotically safe gravity, as a function of r, for varying values of the parameter of BH η and the angular momentum. It is noted that the effective force acting on the particles has the same behavior for both the parameters η and the angular momentum. The effective force is small when the parameter η or the angular momentum $\mathcal{L}$ has small values, however, the effective force increases when the parameter η or the angular momentum $\mathcal{L}$ increases. When we fix the angular momentum and vary the BH parameter η, the effective force radial profiles coincide as the radial distance r increases. However, for varying values of angular momentum, different radial profiles of effective force can be observed as the radial distance r increases.

We have explored the epicyclic oscillations and fundamental frequencies of test particles moving around a regular BH within asymptotically safe gravity. The BH parameter η is shown to contribute to the shift of the fundamental frequencies of the test particles close to the BH horizon. The particles around Schwarzschild BH have higher frequencies as compared to those particles traveling around regular BH within asymptotically safe gravity. We also examine the frequency of the periastron and the effects of the BH parameter on it. We observed that the frequency of the periastron decreases as the parameter η increases and also decreases with increasing radial distance r.

We have studied the collisions of particles and the center of mass energy around non-rotating regular BH within asymptotically safe gravity. It is observed that the center of mass energy is high near the BH event horizon; however, the center of mass energy is reduced as we move away from the BH. For small values of the BH parameter η, the center of mass energy is low, the center of mass energy increases as we increase the value of the BH parameter η. We have also shown the behavior of the center-of-mass energy for different values of angular momentum of one of the colliding particles for three different cases, i.e. $\eta < \eta_{cr}$ and $\eta = \eta_{cr}$. It is interesting to note that the behavior of the BH parameter η on the center of mass energy and the behavior of the angular momentum of one of the colliding particles on the center of mass energy are opposite. In contrast to the BH parameter η, the energy of the center of mass decreases as the angular momentum values increase. High energy can be produced for the case $\eta < \eta_{cr}$, as compared to the cases $\eta = \eta_{cr}$.

Also, we have studied the radius of photon sphere and shadow of the regular black hole in the background of asymptotically safe gravity. Our analysis confirms that an increase in the parameter η leads to a decrease in both the photon sphere radius and the shadow radius. Using EHT collaboration data, we obtained a constraint on the parameter η for the supermassive black hole Sgr A* and M87*. Consequently, the regular BH parameter η has been constrained to $0 < \eta/M^2 < 0.4565$ for both Sgr A* and M87*.

Acknowledgements The authors extend their appreciation to the Deanship of Research and Graduate Studies at King Khalid University for funding this work through the Large Research Project under grant number RGP2/5/46.

Data Availability Statement This manuscript has no associated data or the data will not be deposited. (There is no observational data related to this article. The necessary calculations and graphic discussion can be made available on request.)

Code Availability Statement This manuscript has no associated code/software. [Authors' comment: Code/Software sharing not applicable to this article as no code/software was generated or analysed during the current study.]

Funded by SCOAP[3].

References

1. J. Bardeen, in *Proceedings of the 5th International Conference on Gravitation and the Theory of Relativity*, p. 87 (1968)
2. E. Ayón-Beato, A. García, Phys. Rev. Lett. **80**, 5056 (1998). https://doi.org/10.1103/PhysRevLett.80.5056. arXiv:gr-qc/9911046
3. S.A. Hayward, Phys. Rev. Lett. **96**, 031103 (2006). https://doi.org/10.1103/PhysRevLett.96.031103. arXiv:gr-qc/0506126
4. Z.-Y. Fan, X. Wang, Phys. Rev. D **94**, 124027 (2016). https://doi.org/10.1103/PhysRevD.94.124027. arXiv:1610.02636 [gr-qc]
5. A. Davlataliev, B. Narzilloev, I. Hussain, A. Abdujabbarov, B. Ahmedov, (2024). arXiv:2412.09464 [gr-qc]
6. J. Ovalle, R. Casadio, A. Giusti, Phys. Lett. B **844**, 138085 (2023). https://doi.org/10.1016/j.physletb.2023.138085. arXiv:2304.03263 [gr-qc]
7. J.T.S.S. Junior, F.S.N. Lobo, M.E. Rodrigues, Class. Quantum Gravity **41**, 055012 (2024). https://doi.org/10.1088/1361-6382/ad210e. arXiv:2310.19508 [gr-qc]
8. A. Bakopoulos, C. Charmousis, P. Kanti, N. Lecoeur, T. Nakas, Phys. Rev. D **109**, 024032 (2024). https://doi.org/10.1103/PhysRevD.109.024032. arXiv:2310.11919 [gr-qc]
9. B. Turimov, A. Davlataliev, Y. Usmanov, S. Karshiboev, P. Tadjimuratov, Eur. Phys. J. C **84**, 1098 (2024). https://doi.org/10.1140/epjc/s10052-024-13426-w
10. B. Turimov, A. Davlataliev, B. Ahmedov, Z. Stuchlík, Chin. J. Phys. **94**, 807 (2025). https://doi.org/10.1016/j.cjph.2024.09.030. arXiv:2409.14110 [gr-qc]
11. B. Turimov, A. Davlataliev, A. Abdujabbarov, B. Ahmedov, Phys. Rev. D **110**, 084053 (2024). https://doi.org/10.1103/PhysRevD.110.084053. arXiv:2409.06225 [gr-qc]
12. C.G. Böhmer, K. Vandersloot, Phys. Rev. D **76**, 104030 (2007). https://doi.org/10.1103/PhysRevD.76.104030. arXiv:0709.2129 [gr-qc]
13. L. Modesto, P. Nicolini, Phys. Rev. D **82**, 104035 (2010). https://doi.org/10.1103/PhysRevD.82.104035. arXiv:1005.5605 [gr-qc]
14. A. Bonanno, D. Malafarina, A. Panassiti, Phys. Rev. Lett. **132**, 031401 (2024). https://doi.org/10.1103/PhysRevLett.132.031401. arXiv:2308.10890 [gr-qc]
15. R. Carballo-Rubio, F. Di Filippo, S. Liberati, M. Visser, Phys. Rev. D **101**, 084047 (2020). https://doi.org/10.1103/PhysRevD.101.084047. arXiv:1911.11200 [gr-qc]
16. A. Bonanno, M. Reuter, Phys. Rev. D **62**, 043008 (2000). https://doi.org/10.1103/PhysRevD.62.043008. arXiv:hep-th/0002196
17. A. Bonanno, D. Malafarina, A. Panassiti, Phys. Rev. Lett. **132**, 031401 (2024). https://doi.org/10.1103/PhysRevLett.132.031401. arXiv:2308.10890 [gr-qc]
18. K. Akiyama et al. (Event Horizon Telescope Collaboration), Astrophys. J. **875**, L1 (2019). https://doi.org/10.3847/2041-8213/ab0ec7. arXiv:1906.11238 [astro-ph.GA]
19. B.P. Abbott et al. (LIGO Scientific Collaboration and Virgo Collaboration), Phys. Rev. Lett. **116**, 061102 (2016). https://doi.org/10.1103/PhysRevLett.116.061102
20. K.G. Arun et al., Living Rev. Relativ. **25**, 4 (2022). https://doi.org/10.1007/s41114-022-00036-9. arXiv:2205.01597 [gr-qc]
21. A. Flachi, J.P.S. Lemos, Phys. Rev. D **87**, 024034 (2013). https://doi.org/10.1103/PhysRevD.87.024034. arXiv:1211.6212 [gr-qc]
22. S. Sau, J.W. Moffat, Phys. Rev. D **107**, 124003 (2023). https://doi.org/10.1103/PhysRevD.107.124003. arXiv:2211.15040 [gr-qc]
23. M. Kološ, M. Shahzadi, Z. Stuchlík, Eur. Phys. J. C **80**, 133 (2020). https://doi.org/10.1140/epjc/s10052-020-7692-5
24. M. Kološ, M. Shahzadi, A. Tursunov, Eur. Phys. J. C **83**, 323 (2023). https://doi.org/10.1140/epjc/s10052-023-11498-8. arXiv:2304.13603 [gr-qc]
25. M. Shahzadi, M. Kološ, R. Saleem, Y. Habib, A. Eduarte-Rojas, Phys. Rev. D **108**, 103006 (2023). https://doi.org/10.1103/PhysRevD.108.103006. arXiv:2310.04514 [gr-qc]
26. M. Kološ, M. Shahzadi, in *Proceedings of RAGtime 23-25: Workshops on Black Holes and Neutron Stars*, ed. by Z. Stuchlik, G. Torok, V. Karas, D. Lancova (2023), pp. 21–27
27. M. Shahzadi, M. Kološ, Z. Stuchlík, Y. Habib, Eur. Phys. J. C **81**, 1067 (2021). https://doi.org/10.1140/epjc/s10052-021-09868-1. arXiv:2104.09640 [astro-ph.HE]
28. M. Shahzadi, M. Kološ, Z. Stuchlík, Y. Habib, Eur. Phys. J. C **82**, 407 (2022). https://doi.org/10.1140/epjc/s10052-022-10347-4. arXiv:2201.04442 [gr-qc]
29. M. Shahzadi, M. Kološ, R. Saleem, Z. Stuchlík, Class. Quantum Gravity **41**, 075014 (2024). https://doi.org/10.1088/1361-6382/ad2e43. arXiv:2309.09712 [gr-qc]
30. A. Davlataliev, J. Rayimbaev, F. Abdulkhamidov, Z. Stuchlik, A. Abdujabbarov, Phys. Dark Univ. **46**, 101590 (2024). https://doi.org/10.1016/j.dark.2024.101590
31. A. Davlataliev, B. Narzilloev, I. Hussain, A. Abdujabbarov, B. Ahmedov, Eur. Phys. J. C **84**, 694 (2024). https://doi.org/10.1140/epjc/s10052-024-13039-3
32. A.M. Hillas, Ann. Rev. Astron. Astrophys. **22**, 425 (1984). https://doi.org/10.1146/annurev.aa.22.090184.002233
33. K.V. Ptitsyna, S.V. Troitsky, Phys. Usp. **53**, 691 (2010). https://doi.org/10.3367/UFNe.0180.201007c.0723. arXiv:0808.0367 [astro-ph]
34. X.-M. Deng, Eur. Phys. J. C **80**, 489 (2020). https://doi.org/10.1140/epjc/s10052-020-8067-7
35. U. Nucamendi, R. Becerril, P. Sheoran, Eur. Phys. J. C **80**, 35 (2020). https://doi.org/10.1140/epjc/s10052-019-7584-8. arXiv:1910.00156 [gr-qc]
36. X.-M. Deng, Phys. Dark Univ. **30**, 100629 (2020). https://doi.org/10.1016/j.dark.2020.100629
37. B. Gao, X.-M. Deng, Eur. Phys. J. C **81**, 983 (2021). https://doi.org/10.1140/epjc/s10052-021-09782-6
38. N. Cruz, M. Olivares, J.R. Villanueva, Class. Quantum Gravity **22**, 1167 (2005). https://doi.org/10.1088/0264-9381/22/6/016. arXiv:gr-qc/0408016
39. S. Shafiq, S. Hussain, M. Ozair, A. Aslam, T. Hussain, Eur. Phys. J. C **80**, 744 (2020). https://doi.org/10.1140/epjc/s10052-020-8314-y. arXiv:2110.13897 [gr-qc]
40. M. Sharif, M. Shahzadi, J. Exp. Theor. Phys. **127**, 491 (2018). https://doi.org/10.1134/S1063776118090182
41. M. Sharif, M. Shahzadi, Eur. Phys. J. C **77**, 363 (2017). https://doi.org/10.1140/epjc/s10052-017-4898-2. arXiv:1705.03058 [gr-qc]
42. J.L. Synge, Mon. Not. Roy. Astron. Soc. **131**, 463 (1966). https://doi.org/10.1093/mnras/131.3.463
43. J.P. Luminet, Astron. Astrophys. **75**, 228 (1979)
44. J.M. Bardeen, in *Black Holes (Les Astres Occlus)*, ed. by C. Dewitt, B.S. Dewitt (1973), pp. 241–289
45. R. Kumar, A. Kumar, S.G. Ghosh, Astrophys. J. **896**, 89 (2020). https://doi.org/10.3847/1538-4357/ab8c4a. arXiv:2006.09869 [gr-qc]
46. M. Afrin, S. Vagnozzi, S.G. Ghosh, Astrophys. J. **944**, 149 (2023). https://doi.org/10.3847/1538-4357/acb334. arXiv:2209.12584 [gr-qc]

47. B. Puliçe, R.C. Pantig, A. Övgün, D. Demir, Class. Quantum Gravity **40**, 195003 (2023). https://doi.org/10.1088/1361-6382/acf08c. arXiv:2308.08415 [gr-qc]
48. Z. Yan, X. Zhang, M. Wan, C. Wu, Eur. Phys. J. Plus **138**, 377 (2023). https://doi.org/10.1140/epjp/s13360-023-03978-3. arXiv:2304.07952 [gr-qc]
49. E. Ghorani, B. Puliçe, F. Atamurotov, J. Rayimbaev, A. Abdujabbarov, D. Demir, Eur. Phys. J. C **83**, 318 (2023). https://doi.org/10.1140/epjc/s10052-023-11490-2. arXiv:2304.03660 [gr-qc]
50. F. Atamurotov, I. Hussain, G. Mustafa, A. Övgün, Chin. Phys. C **47**, 025102 (2023). https://doi.org/10.1088/1674-1137/ac9fbb
51. R.A. Konoplya, Phys. Lett. B **804**, 135363 (2020). https://doi.org/10.1016/j.physletb.2020.135363. arXiv:1912.10582 [gr-qc]
52. Z. Younsi, A. Zhidenko, L. Rezzolla, R. Konoplya, Y. Mizuno, Phys. Rev. D **94**, 084025 (2016). https://doi.org/10.1103/PhysRevD.94.084025. arXiv:1607.05767 [gr-qc]
53. R.A. Konoplya, T. Pappas, A. Zhidenko, Phys. Rev. D **101**, 044054 (2020). https://doi.org/10.1103/PhysRevD.101.044054. arXiv:1907.10112 [gr-qc]
54. F. Atamurotov, F. Sarikulov, S.G. Ghosh, G. Mustafa, Phys. Dark Univ. **46**, 101625 (2024). https://doi.org/10.1016/j.dark.2024.101625
55. N.U. Molla, H. Chaudhary, G. Mustafa, F. Atamurotov, U. Debnath, D. Arora, Eur. Phys. J. C **84**, 574 (2024). https://doi.org/10.1140/epjc/s10052-024-12917-0. arXiv:2310.14234 [gr-qc]
56. V. Perlick, O. Y. Tsupko, Phys. Rep. **947**, 1 (2022). https://doi.org/10.1016/j.physrep.2021.10.004. arXiv:2105.07101 [gr-qc]
57. G. Mustafa, F. Atamurotov, I. Hussain, S. Shaymatov, A. Övgün, Chin. Phys. C **46**, 125107 (2022). https://doi.org/10.1088/1674-1137/ac917f. arXiv:2207.07608 [gr-qc]
58. R.C. Pantig, L. Mastrototaro, G. Lambiase, A. Övgün, Eur. Phys. J. C **82**, 1155 (2022). https://doi.org/10.1140/epjc/s10052-022-11125-y. arXiv:2208.06664 [gr-qc]
59. I. Banerjee, S. Sau, S. SenGupta, JCAP **2022**, 066 (2022). https://doi.org/10.1088/1475-7516/2022/09/066. arXiv:2206.12125 [gr-qc]
60. N.U. Molla, U. Debnath, Ann. Phys. **453**, 169304 (2023). https://doi.org/10.1016/j.aop.2023.169304. arXiv:2212.02104 [gr-qc]
61. F. Atamurotov, I. Hussain, G. Mustafa, K. Jusufi, Eur. Phys. J. C **82**, 831 (2022). https://doi.org/10.1140/epjc/s10052-022-10782-3. arXiv:2209.01652 [gr-qc]
62. F. Atamurotov, U. Papnoi, K. Jusufi, Class. Quantum Gravity **39**, 025014 (2022). https://doi.org/10.1088/1361-6382/ac3e76. arXiv:2104.14898 [gr-qc]
63. D. Arora, N.U. Molla, H. Chaudhary, U. Debnath, F. Atamurotov, G. Mustafa, Eur. Phys. J. C **83**, 995 (2023). https://doi.org/10.1140/epjc/s10052-023-12185-4. arXiv:2308.13901 [gr-qc]
64. M. Bañados, J. Silk, S.M. West, Phys. Rev. Lett. **103**, 111102 (2009). https://doi.org/10.1103/PhysRevLett.103.111102. arXiv:0909.0169 [hep-ph]
65. A. Baushev, Int. J. Mod. Phys. D **18**, 1195 (2009). https://doi.org/10.1142/S0218271809014509. arXiv:0805.0124 [astro-ph]
66. M.A. Markov, V.F. Mukhanov, Nuovo Cimento B Serie **86B**, 97 (1985). https://doi.org/10.1007/BF02732276
67. M. Reuter, Phys. Rev. D **57**, 971 (1998). https://doi.org/10.1103/PhysRevD.57.971. arXiv:hep-th/9605030
68. A. Bonanno, T. Denz, J.M. Pawlowski, M. Reichert, SciPost Phys. **12**, 001 (2022). https://doi.org/10.21468/SciPostPhys.12.1.001. arXiv:2102.02217 [hep-th]
69. L. Stella, M. Vietri, Astrophy. J. Lett. **492**, L59 (1998). https://doi.org/10.1086/311075
70. L. Stella, M. Vietri, Phy. Rev. Lett. **82**, 17 (1999). https://doi.org/10.1103/PhysRevLett.82.17
71. W.K.M.A. Abramowicz, Astron. Astrophys. **404**, L21 (2003). https://doi.org/10.1051/0004-6361:20030749
72. G. Török, M.A. Abramowicz, W. Kluźniak, Z. Stuchlík, Astron. Astrophys. **436**, 1 (2005). https://doi.org/10.1051/0004-6361:20042491
73. D. Foreman-Mackey, D.W. Hogg, D. Lang, J. Goodman, Publ. Astron. Soc. Pac. **125**, 306 (2013). https://doi.org/10.1086/670067. arXiv:1202.3665 [astro-ph.IM]
74. C. Liu, H. Siew, T. Zhu, Q. Wu, Y. Sun, Y. Zhao, H. Xu, J. Cosmol. Astropart. Phys. **11**, 096 (2023). https://doi.org/10.1088/1475-7516/2023/11/096. arXiv:2305.12323 [gr-qc]
75. F. Abdulkhamidov, P. Nedkova, J. Rayimbaev, J. Kunz, B. Ahmedov, Phys. Rev. D **109**, 104074 (2024). https://doi.org/10.1103/PhysRevD.109.104074. arXiv:2403.08356 [gr-qc]
76. A. Davlataliev, F. Atamurotov, A. Abdujabbarov, N. Juraeva, V. Khamidov, Phys. Dark Univ. **46**, 101603 (2024). https://doi.org/10.1016/j.dark.2024.101603
77. G. Mustafa, E. Demir, A. Davlataliev, H. Chaudhary, F. Atamurotov, E. Güdekli, Phys. Dark Univ. **46**, 101644 (2024). https://doi.org/10.1016/j.dark.2024.101644
78. A. Davlataliev, B. Narzilloev, I. Hussain, A. Abdujabbarov, B. Ahmedov, Phys. Dark Univ. **46**, 101569 (2024). https://doi.org/10.1016/j.dark.2024.101569
79. H. Hoshimov, A. Davlataliev, F. Atamurotov, A. Abdujabbarov, A. Övgün, JHEAp **45**, 306 (2025). https://doi.org/10.1016/j.jheap.2024.12.012
80. S.E. Motta, T. Belloni, L. Stella, G. Pappas, J. Casares, A.T. Muñoz-Darias, M.A.P. Torres, I.V. Yanes-Rizo, Mon. Not. Roy. Astron. Soc. **517**(1), 1469–1475 (2022). https://doi.org/10.1093/mnras/stac2142. arXiv:2209.10376 [astro-ph.HE]
81. S. Vagnozzi et al., Class. Quantum Gravity **40**, 165007 (2023). https://doi.org/10.1088/1361-6382/acd97b. arXiv:2205.07787 [gr-qc]
82. K. Akiyama et al., Astrophys. J. Lett. **930**, L12 (2022). https://doi.org/10.3847/2041-8213/ac6674
83. A. Urmanov, H. Chakrabarty, D. Malafarina, **85**, 1 (2025). https://doi.org/10.48550/arXiv.2504.12072. arXiv:2504.12072 [gr-qc]